Applied Surface Science 441 (2018) 341–346

Contents lists available at ScienceDirect

Applied Surface Science

journal homepage: www.elsevier.com/locate/apsusc

Full Length Article

Rabi like angular splitting in Surface Plasmon Polariton – Exciton interaction in ATR configuration

Heba Hassan [a], T. Abdallah [a], S. Negm [b], H. Talaat [a,*]

[a] Physics Department, Faculty of Science, Ain Shams University, Abbassia, Cairo, Egypt
[b] Department of Mathematical and Physical Engineering, Faculty of Engineering (Shoubra), Banha University, Cairo, Egypt

ARTICLE INFO

Article history:
Received 12 November 2017
Revised 31 January 2018
Accepted 2 February 2018
Available online 6 February 2018

Keywords:
Surface Plasmon Polaritons (SPPs)
Exciton generation in semiconductor QDs
Plasmon-exciton coupling
Rabi splitting

ABSTRACT

We have studied the coupling of propagating Surface Plasmon Polaritons (SPP) on silver films and excitons in CdS quantum dots (QDs). We employed the Kretschmann-Raether configuration of the attenuated total reflection (ATR) to propagate the SPP on silver film of thickness 47.5 nm at three different wavelengths. The CdS QD have been chemically synthesized with particular size such that its exciton of energy would resonate with SPP. High resolution transmission electron microscopy (HRTEM) and scan tunneling microscopy (STM) were used to measure the corresponding QDs size and confirm its shape. Further confirmation of the size has been performed by the effective mass approximation (EMA) model utilizing the band gap of the prepared QDs. The band gaps have been measured through UV–vis absorption spectra as well as scan tunneling spectroscopy (STS). The coupling has been observed as two branching dips in the ATR spectra indicating Rabi like splitting. To the best of our knowledge, this is the first time that Rabi interaction is directly observed in an ATR angular spectra. This observation is attributed to the use a high resolution angular scan (±0.005°), in addition to the Doppler width of the laser line as well as the energy distribution of the excitons. The effect of three different linker molecules (TOPO, HDA), (Pyridine) and (Tri-butylamine) as surface ligands, on SPP-Exciton interaction has been examined.

1. Introduction

The interaction between plasmons in metals and excitons in semiconductor quantum dots (QDs) have been studied extensively, both theoretically and experimentally over the past two decades [1–4], as a mean of modifying their photophysical properties. Potential novel applications in nanoscale devices include lasers [5], optical switches [6], sensors [7], light-emitting diodes [8–9], and photovoltaic solar cells [10]. Usually there are two configurations to generate the surface plasmon-polaritons (SPPs), in the Kretschmann configuration of attenuated total reflection (ATR) spectra. Either, varying the incident frequency (ω) at a fixed angle of incidence through the prism θ or varying the angle of incidence at a fixed photon energy. The frequency ω and the wavevector of the incident electromagnetic wave k_x, are connected by "ATR scan-line" [11]; $k_x = \frac{w}{c}\sqrt{\varepsilon}\sin\theta$ where c is the velocity of light in vacuum, ε is the dielectric constant for the prism, θ is the internal angle of incidence in the prism.

The mixing of plasmons and exciton modes leads to the formation of plasmon-exciton mixed states, that has been observed in both organic [12–14] and inorganic systems [15]. However, such an interaction can be divided into weak and strong coupling regimes, in the weak coupling regime, wave functions and electromagnetic modes of plasmons and excitons are unperturbed. The strong coupling occurs when surface plasmon resonate with the QDs exciton and the excitation energy oscillates between the plasmonic – excitionic system, called Rabi oscillation. This leads to anti-crossing and splittingof energy levels that is normally observed in frequency scan spectra [16]. Such scan, has been studied theoretically by Bludov and Vasilevskiy [11] and experimentally by Davis [17]. In their work, the reflectivity as a function of frequency R (w), exhibits two minima with approximately equal depth at an angle of incidence close to $\theta_i = \theta_{ATR}$ where θ_{ATR} is the angle of incidence corresponding to generation of SPP. indicating max coupling of electromagnetic energy. At other angles of incidence, one of the minima is significantly deeper than the other as a result of strong coupling either to the plasmon or exciton [11]. The shift between the two minima represents the Rabi splitting.

Most of the previous works [16–20], of surface plasmon and exciton interaction have been focused on localized surface plasmons (LSP) generated in metal nanoparticles and exciton in

* Corresponding author at: Physics Department, Ain Shams University, Room 220, Khalifa El-maamoon St., Abbassia, Cairo, Egypt.
E-mail address: hassantalaat@hotmail.com (H. Talaat).

https://doi.org/10.1016/j.apsusc.2018.02.020
0169-4332/

semiconductor Quantum dots and the hybridization was named Plexciton [18]. In this work, we present an experimental demonstration of energy coupling that occurs between propagating SPP on silver thin film and excitons confined in CdS semiconductor QDs using the angular scan configuration of ATR. The coupling was designed to be observed using SPP generated as the actual probe. The use of silver is due to its lower intrinsic losses resulting in narrow SP resonance in the visible spectrum. On the other hand, semiconductor quantum dots have discrete energy levels that can be tuned by changing the size of QD.

The objective here is to investigate the resonant interaction of exciton in a particular dimension of CdS QD with SPP on silver film. Since the QD exciton energy can be tuned by controlling the size, the precise determination of the size is of fundamental importance to our experiment. Therefore, high resolution transmission electron microscope (HR-TEM) and scan tunneling microscopy (STM) have been used to determine and confirm the QD size. Also, the effective mass approximation (EMA) [21] has been applied to the optical spectra of the nanoparticles to estimate the QDs size. According to this model, taking into account the effects of valence band mixing and the e-h coulomb interaction, the nanocrystal (NC) band gap is given by the following relation;

$$E_g(NC) = E_g(Bulk) + \frac{h^2\pi^2}{2\mu D^2} - \frac{1.8e^2}{2\pi\varepsilon\varepsilon_o D} \quad (1)$$

where E_g(NC) is the lowest energy for electronic transition states for nanocrystal, Eg (bulk) is the energy band gap for bulk CdS (2.42 eV), D is the diameter of nanoparticles, μ is the reduced mass of electron and hole, e is the electron charge, and ε is the dielectric constant for CdS crystal. Hence the diameter of the nanoparticles was determined.

Furthermore, the effect of the nanoscale distance (between the silver film and the CdS QDs), on the SPP – exciton coupling has been investigated. This was accomplished by using different surface ligands (surfactant molecules) of the synthesized CdS nanocrystals which are trioctylphosphine oxide, hexadecylamine $OP(C_8H_{17})_3$, $C_{16}H_{35}N$, Pyridine (C_5H_5N), and tri-butylamine ($C_{12}H_{27}N$).

2. Experimental

2.1. Materials

The following materials were purchased, cadmium oxide (CdO, Aldrich), trioctylphosphine oxide (TOPO, Aldrich), sulfur (Aldrich), trioctylphosphine (TOP, Fluka), oleic acid (Aldrich), hexadecylamine (HDA, Fluka), Pyridine (Sigma Aldrich), tri-butylamine (Sigma Aldrich), Toluene (Sigma) and methanol (Sigma).

2.2. Preparation of CdS QDs

2.2.1. CdS capped with TOPO, HDA

0.3 g of CdO was dissolved in 4 ml oleic acid until colorless, and then a mixture of 2 g of TOPO and 2 g of HDA was added and held at 170 °C for 5 min to get a clear solution. A 0.3 g of sulfur (S) was dissolved in 6 mL of TOP, this solution was quickly injected into the prepared Cd source, and the temperature was raised to 130 °C for the growth of CdS QDs. After 10-min, quenching by Toluene to stop the reaction. The particles were washed three times with methanol and re-dispersed in toluene [22].

2.2.2. CdS capped with pyridine (first surface modification)

0.1 gm of CdS capped with TOPO, HDA was treated with 10 ml pyridine and left overnight at 70 °C, then quenched by methanol and centrifuged in toluene.

2.2.3. CdS capped with tri-butylamine (second surface modification)

0.1 gm of CdS capped with pyridine was added to 10 ml of tributylamine at 70 °C and left overnight and then quenched by toluene and centrifuged in methanol.

The size of the CdS QD was determined directly by HR-TEM and STM and indirectly using the EMA model by measuring E_g(NC) through UV–vis spectra as well as scan tunneling spectroscopy (STS). The presence of the surfactant molecules on QDs was confirmed by the Fourier transform infrared spectroscopy (FTIR) spectroscopy.

Samples for ATR measurements were prepared by spin coating of 100 μl of CdS with the capping reagents on Ag film of 47.5 nm thick at speed of 3000 rpm; This was repeated for each of the three surfactants.

3. Results and discussions

HR-TEM images for CdS QDs capped with TOPO, HDA is shown in Fig. 1(a–c). It is seen from Fig. 1(a) that the size of the QDs is (∼3.5 nm). Atomic planes are shown in Fig. 1(b) with an interplanar distance of 3.367 Å. This is in good agreement with the distance 3.36 Å between planes (1 1 1) in hawleyite [23]. This small difference can be attributed to distortions of the lattice due the nanometric particle size [23]. This formation is explicitly confirmed by the selected area of electron diffraction pattern (SAED) shown in Fig. 1c, giving interplanar spacings of 3.367 Å, 2.06 Å and 1.75 Å which match with distances between planes (1 1 1), (2 2 0) and (3 1 1) respectively of cubic CdS in hawleyite (ICDD 0010-0454). Fig. 2 shows STM image, giving the diameter of CdS capped with TOPO, HDA around 3.2 ± 0.18 nm. Fig. 3 shows the UV–vis absorption spectra for CdS QDs, for different capping materials as indicated. It is obvious that all spectra show the same behavior with an equal absorption peak around 458 ± 1 nm, indicating the same excitonic energy (≈2.7 eV) for the all samples. STS measurements shown in Fig. 4 also confirmed the band gap of the CdS QDs as (≈2.56 eV). The calculated value of the size of CdS QDs (≈3 nm) by applying EMA model (Eq. (1)) is comparable to those measured by HRTEM and STM. As was mentioned before, the size was carefully selected during the synthesis to have excitonic energy matching the SPP in the Ag film at 448 nm.

The ATR spectrum for bare Ag film with thickness 47.5 nm is shown in Fig. 5a (dashed line), where θ_{ATR} is 46.93° due to generation of the SPP at an incident p-polarized laser light of 448 nm. To minimize any alteration, the same Ag film was coated with QD using spin coater to be able to accurately observe the coupling of the SPP in the Ag film and exciton in the CdS QD. The selected CdS QD size has an absorption peak at (458 nm) that is close to the SPP in the Ag film (448 nm). Fig. 5a (solid line) shows a dip split, one at about 46.98° and the second at 48.2°. Moreover, the width of the ATR spectra is increased due to the overlap of the two excitations and loading losses. In this case of employing the angular scan ATR, the small dip splitting in the angular spectra is an indication of a weak coupling between SPP and QDs' exciton. To test this evidence, the ATR of other two films of the same thickness were first plotted as bare films and then plotted after coating with QD CdS. The spectra were then carried out at two wavelengths 532 nm and 632 nm that are well separated from the exciton. Fig. 5b shows the ATR spectra of bare Ag (dashed line) and coated film (solid line) at an incident wavelength 532 nm. The bare film has θ_{ATR} at 44.5° while that of the coated film is 44.6°. This expected small shift of the angle results from loading the surface as well as the change of the dielectric at metal surface. Similar result (single dip at 43.85°) has been obtained when using 632 nm as an incident wavelength on the coated film as shown in Fig. 5c (solid line). These results show that the appearance of the

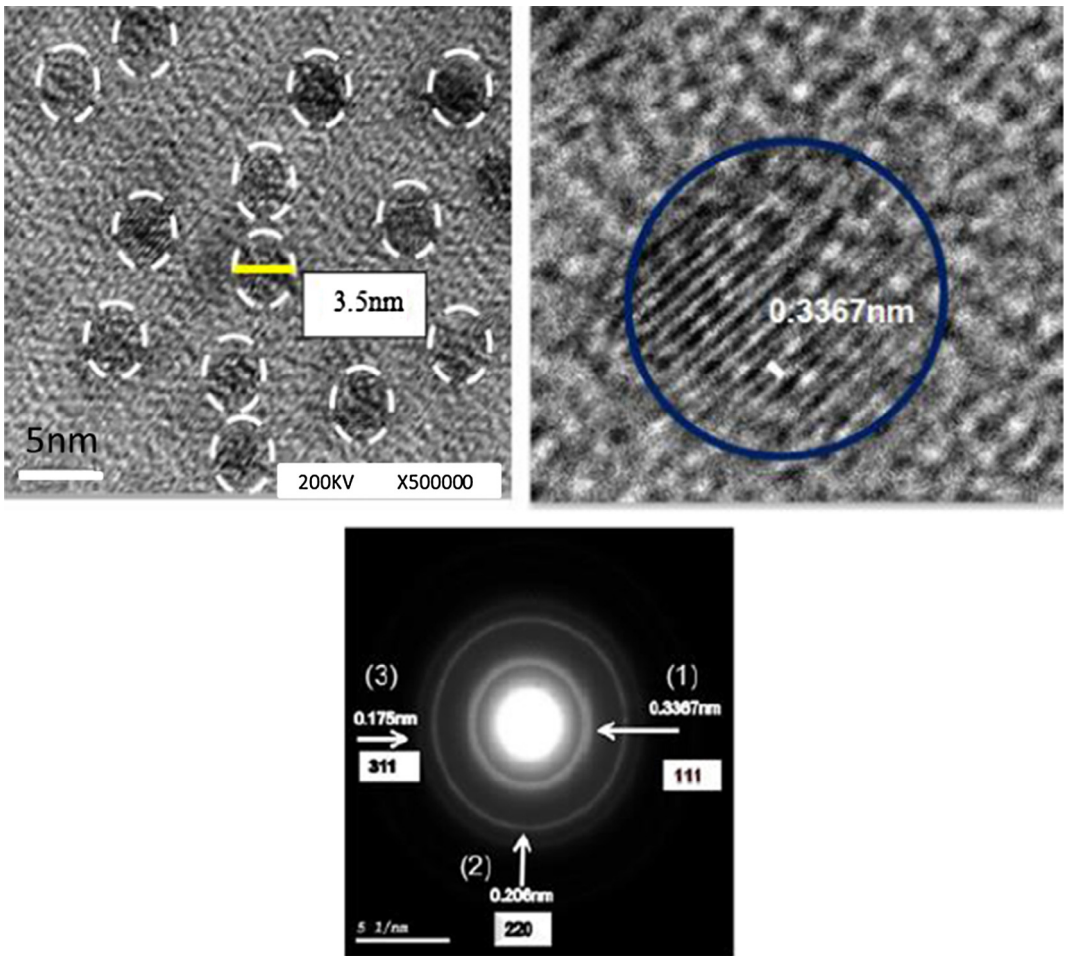

Fig. 1. (a) HRTEM image of CdS QDs capped with TOPO, HAD and (b) an enlarged HRTEM image of CdS NP that is surrounded by the circle. (c) SAED for CdS QDs capped with TOPO, HAD and each plane corresponding to d spacings.

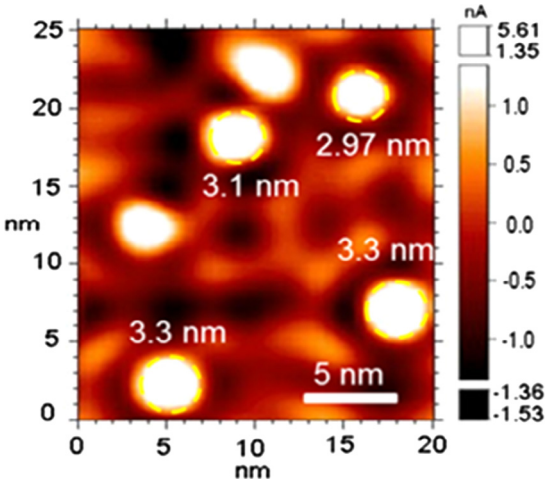

Fig. 2. STM image for CdS QDs capping Topo, HDA.

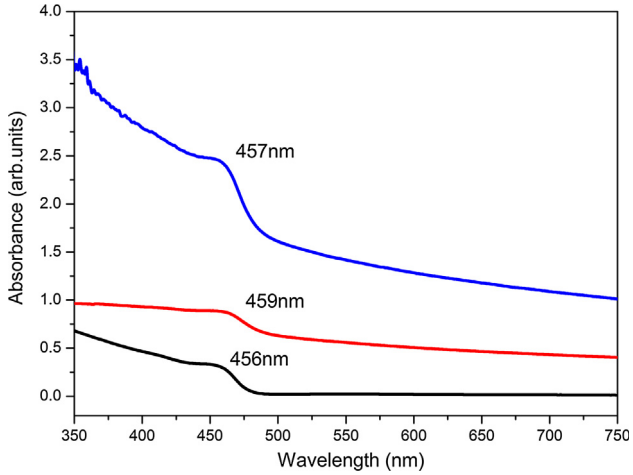

Fig. 3. (a) UV–vis for CdS QDs capped with TOPO, HAD (black color), (b). UV–vis for CdS QDs capped with pyridine (blue color). (c). UV–vis for CdS QDs capped with Tri-Butylamine (red color). (For interpretation of the references to colour in this figure legend, the reader is referred to the web version of this article.)

two branching dips in the ATR spectra occurs only when the SPP energy is comparable to the exciton energy of QDs. We attribute this result to Rabi splitting in the ATR angular scan.

Such weak coupling can be ascribed to the energy overlap of the linewidths of the coupled states [24] be caused by the Doppler width of the used laser beam (inexpensive commercial lasers) and the distribution of the exciton energy of the CdS QD. The ability to measure this weak coupling in a single angular scan that was not observed before may be due to the use of a turn table with an

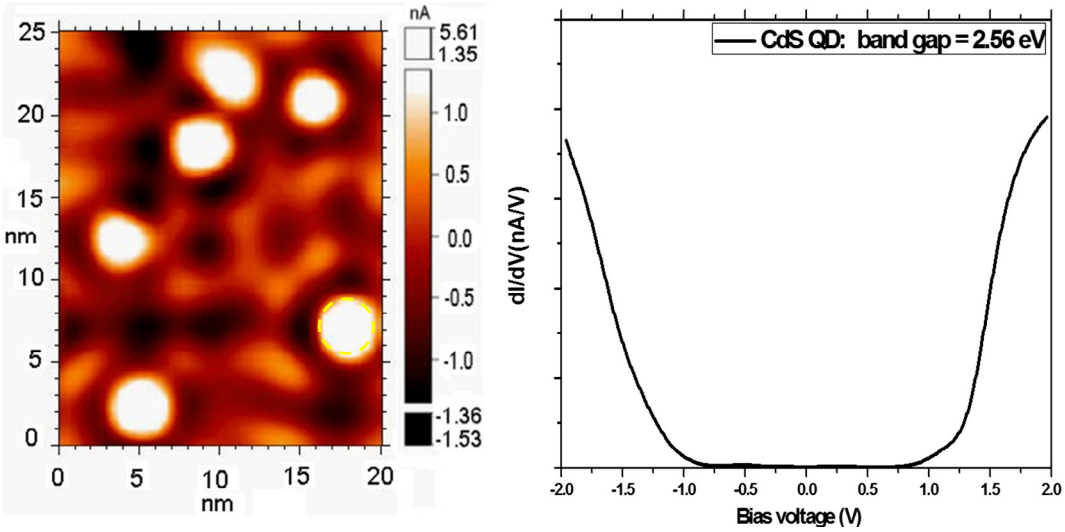

Fig. 4. The STS average tunneling spectrum for the CdS NPs capped with TOPO, HDA.

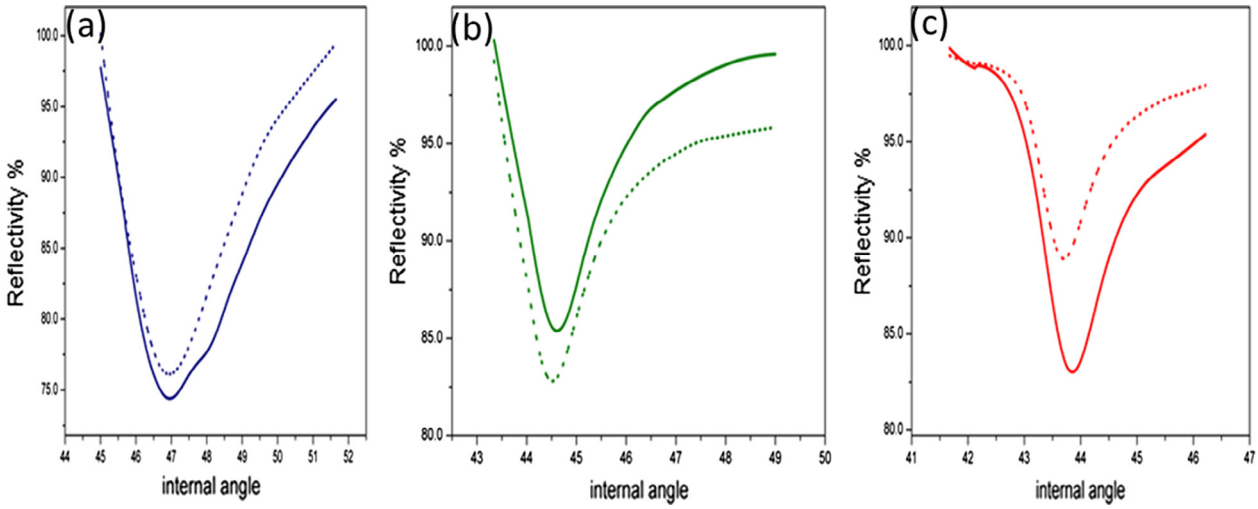

Fig. 5. The ATR spectra of the bare Ag film of thickness 47.5 nm (dashed line) and Ag film covered with CdS capped with (TOPO, HDA) QDs (solid line) at an incident laser light (a) 0.448 nm, (b) 532 nm, (c) 632 nm.

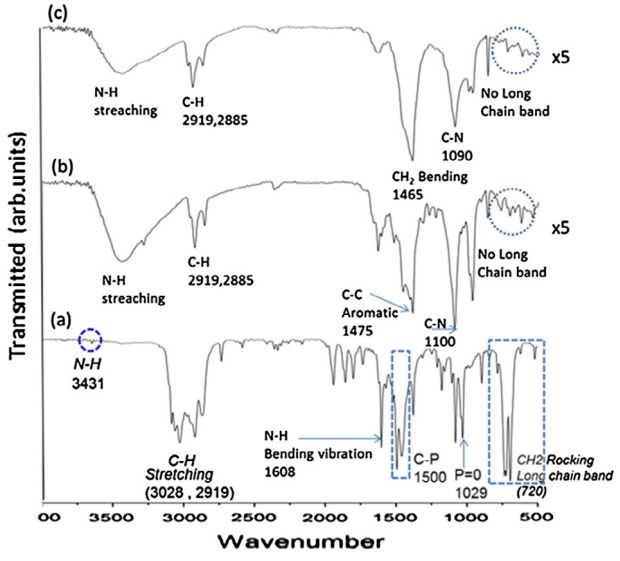

Fig. 6. FTIR for (a). CdS capped with TOPO, HDA, (b) CdS capped Pyridine, (c) CdS capped with Tri-butylamine.

angular resolution of ±0.005 which made this observation possible. For further confirmation of this observation, the above scheme with TOPO, HDA as a surfactant was repeated with other two surfactants Pyridine and Tri-butylamine.

The spin coating of the Ag film with CdS QD capped with surfactant introduces a separation between the CdS QD and the Ag film surface that could be estimated to equal the length of the surfactant molecule. Such a distance has been approximated from the molecular volume of the surfactant. In the case CdS capped with TOPO, HDA such separation is taken as 0.9 nm. Surface modification of CdS QDs by (TOPO, HDA) was confirmed using FTIR spectra as shown in Fig. 6(a). More than one characteristic bands of TOPO appear, for instance the band at 3028 cm^{-1} which is the dissymmetric stretching vibration of CH_3, and the dissymmetric and symmetric stretching vibrations of CH_2 at 2919 and 2865 cm^{-1} respectively [25–29]. Also, the weak N-H band (at 3431 cm^{-1}) due to the presence HDA (aliphatic amines) is hardly seen because the amine group on the HDA molecule was bound to the surface of the nanocrystal [25,30]. FTIR spectra of the QDs capped with the other two different ligands (Pyridine) and (Tri-butylamine) are shown in Fig. 6(b and c) respectively. Fig. 6(b) shows the N-H

stretching band due to the pyridine (aromatic amines), while the C-H and C-P bands are largely decreased as a result of the decrease in chain and remnant traces of the TOPO surfactant respectively. Fig. 6c shows slight decrease in the N-H band due to the relatively smaller ratio of N to C-H in tri-butylamine as compared to pyridine. This also leads to a slight increase in the amplitude of the C-H band. The spectra (b) and (c) have been magnified 5 times to compare to spectrum (a).

Fig. 7a shows the ATR spectra for the bare Ag film (dashed line) and the coated Ag film (solid line) using 448 nm in case of using pyridine as a QDs surfactant. The spectrum shows two dips that are clearly seen. This two dips are closer than the case of TOPO, HDA. Single dip has been obtained when using both 532 nm and 632 nm as shown in Fig. 7(b and c) respectively. This indicates that no coupling between the SPP and possible exciton in QDs. Also, Fig. 8a shows the two dips in case of Tri-butylamine as a surfactant when using 448 nm. The dips are clearer than the case of TOPO, HDA ATR. Again, there is no evidence of coupling at the laser wavelengths 532 nm and 632 nm as shown in Fig. 8(b and c) where the plasmon energy is further from possible exciton. The lengths of surfactants are 0.51 nm, 0.547 for pyridine and Tri-butylamine respectively. These results confirm the angular splitting in ATR angular scan configuration at SPP-exciton coupling and reveal that the strength of the coupling varies with the distance between the QDs and the metal surface.

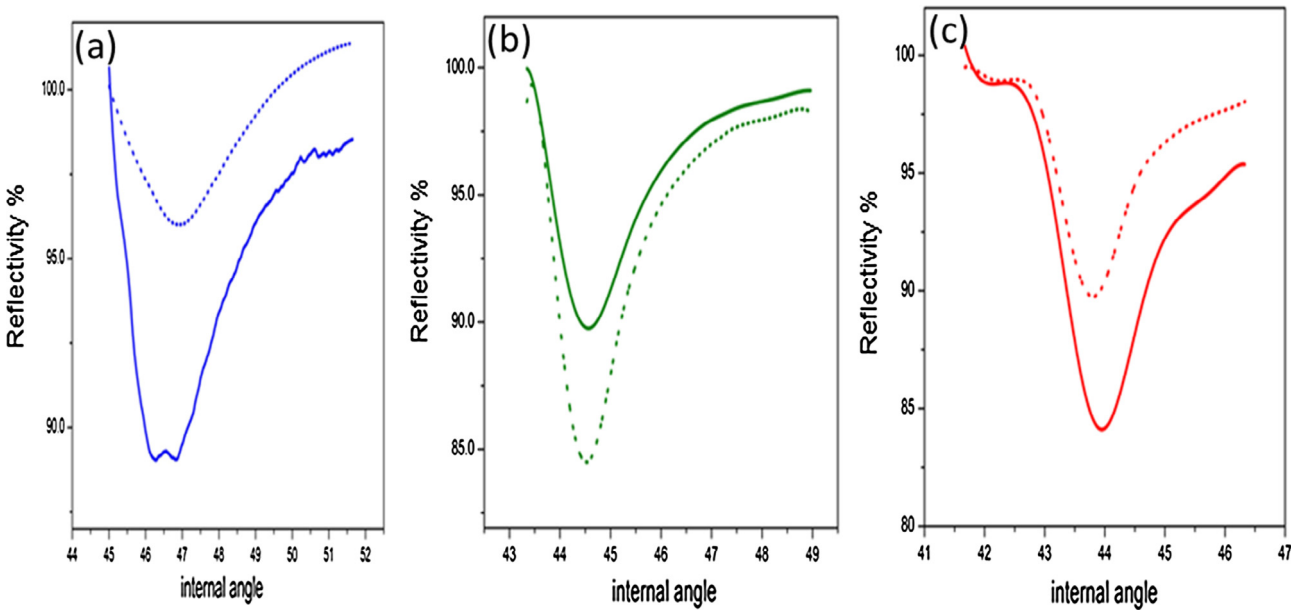

Fig. 7. The ATR spectra of the bare Ag film of thickness 47.5 nm (dashed line) and Ag film covered with CdS capped with (Pyridine) QDs (solid line) at an incident laser light (a) 0.448 nm, (b) 532 nm, (c) 632 nm.

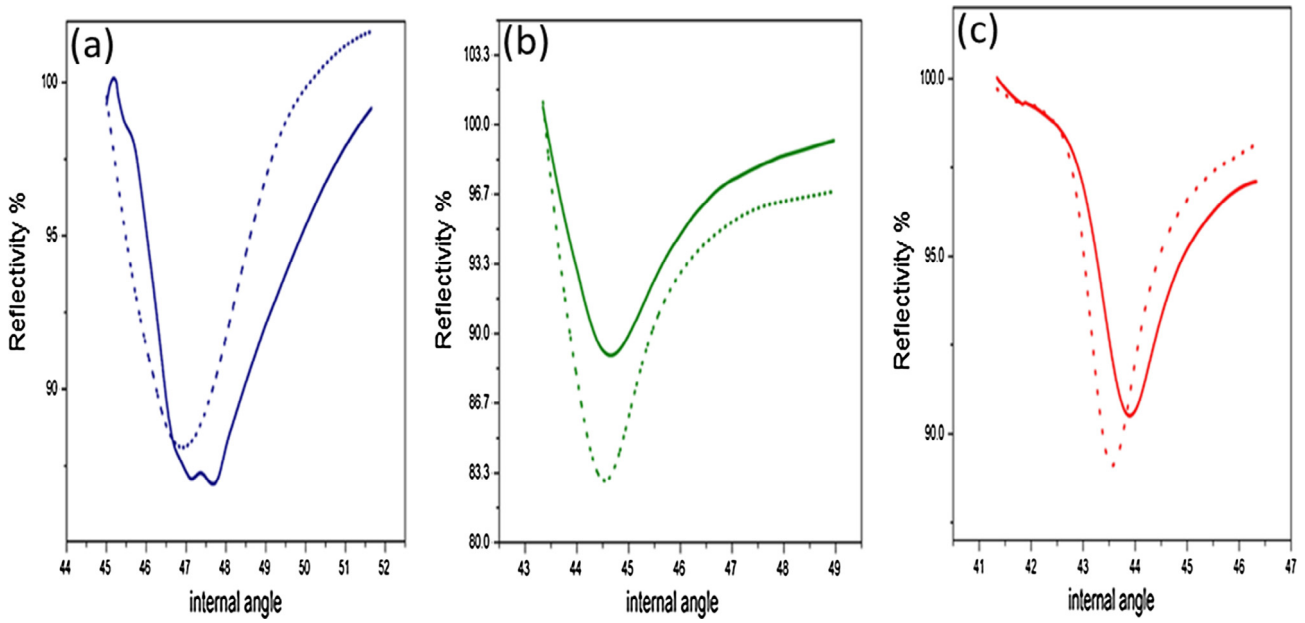

Fig. 8. The ATR spectra of the bare Ag film of thickness 47.5 nm (dashed line) and Ag film covered with CdS capped with (Tri-butylamine) QDs (solid line) at an incident laser light (a) 0.448 nm, (b) 532 nm, (c) 632 nm.

4. Conclusion

SPPs on the Ag film of thickness 47.5 nm at the Ag/air interface were generated by the Kretschmann-Raether configuration of the attenuated total reflection (ATR) at wavelengths 448 nm, 532 nm, and 632 nm. A quantum dot of CdS of size ≈3.5 nm was chemically synthesized to have exciton close to the SPP energy at 488 nm incident laser beam. The QDs band gap was measured by STS. Using a high resolution angular scan (±0.005°) ATR, the weak coupling of the propagating SPP in the Ag film and the exciton in QD CdS is detected when SPP and exciton are near resonance. This coupling is observed as a split in the dip in the ATR angular scan and the broadening of the Lorentizan curve. No coupling of the SPP-exciton occurs when the SPP frequency is out of the exciton energy. Furthermore, the results show that the SPP-exciton coupling varied with the length of the QDs surfactant molecules.

Acknowledgment

The generous support of the Egyptian STDF grant ID 3746 is greatly appreciated. The authors thank Prof. T.A. El-Brolosy for helpful discussions.

References

[1] Mahmoud Saad, Tamer Abdallah, Khalid Easawi, Sohair Negm, Hassan Talaat, Interfacial scanning tunneling spectroscopy (STS) of chalcogenide/metal hybrid nanostructure, Appl. Surf. Sci. 337 (15 May 2015) 1–5.
[2] Mohammad Suja, Bishwajit Debnath, Sunayna B. Bashar, Su. Longxing, Roger Lake, Jianlin Liu, Electrically driven plasmon-exciton coupled random lasing in ZnO metal-semiconductor-metal devices, Appl. Surf. Sci. 439 (1) (May 2018) 525–532.
[3] Takayuki Kiba, Kazuki Yanome, Midori Kawamura, Yoshio Abe, Kyung Ho Kim, Junichi Takayama, Akihiro Murayama, Emission enhancement in indium zinc oxide(IZO)/Ag/IZO sandwiched structure due to surface Plasmon resonance of thin Ag film, Appl. Surf. Sci. 389 (15) (December 2016) 906–910.
[4] George R.S. Andrade, Cristiane C. Nascimento, Zenon M. Lima, Erico Teixeira-Neto, Luiz P. Costa, Iara F. Gimenez, Star-shaped ZnO/Ag hybrid nanostructures for enhanced photocatalysis and antibacterial activity, Appl. Surf. Sci. 399 (31) (March 2017) 573–582.
[5] S. Christopoulos, G.B.H. Von Högersthal, A.J.D. Grundy, P.G. Lagoudakis, A.V. Kavokin, J.J. Baumberg G. Christmann, R. Butte, E.Feltin, J.-F. Carlin, N. Grandjean, Phys. Rev. Lett. 98 (2007) 126405.
[6] D. Bajoni, E. Semenova, A. Lemaître, S. Bouchoule, E. Wertz, P. Senellart, S. Barbay, R. Kuszelewicz, J. Bloch, Phys. Rev. Lett. (2008) 266402.
[7] J. Lee, P. Hernandez, J. Lee, A.O. Govorov, N.A. Kotov, Nat. Mater. 6 (2007) 291.
[8] K. Okamoto, I. Niki, A. Shvartser, Y. Narukawa, T. Mukai, A. Scherer, Nat. Matter. 3 (2004) 601.
[9] Nan-Fu Chiu, MaximeLe Ster, Cheng-Du Yang, Ming-Hung Tseng, Feng-Yu Tsai, Interactions between excitation and extraction modes in an organic-based plasmon-emitting diode, Appl. Surf. Sci. 332 (30) (March 2015) 97–104.
[10] D.G. Lidzey DDCB, M.S. Skolnic, S. Lee, E.S. Lee, T.Y. Kim, et al., Effect of annealing treatment on CdS/CIGS thin film solar cells depending on different CdS deposition temperatures, Sol. Energ. Mat. Sol. C. 141 (2015) 299–308.
[11] K.T. Virgili, Y.V. Bludov, M.I. Vasilevskiy, Resonant excitation of confined excitons in nanocrystal quantum dots using surface plasmon-polaritons, J. Phys. Chem. C. 116 (25) (2012) 13738–13744.
[12] D.G. Lidzey, D.D.C. Bradley, M.S. Skolnick, T. Virgili, S. Walker, D.M. Whittaker, Nature 395 (1998) 53.
[13] P.A. Hobson WLB, D.G. Lidzey, G.A. Gehring, D.M. Whittaker MSS, S. Walker, Strong exciton–photon coupling in a low-Q all-metal mirror microcavity, Appl. Phys. Lett. 81 (2002) 3519.
[14] N. Takada TK, D.D.C. Bradley, Polariton emission from polysilane-based organic microcavities, Appl. Phys. Lett. 82 (1812) 2003.
[15] G. Khitrova HMG, M. Kira, S.W. Koch, A. Scherer, Vacuum Rabi splitting in semiconductors, NP 81 (2006).
[16] Y.V. Bludov, VMReoceinqdusp-pTJoPCC-. Exciton– plasmon interactions in metal– semiconductor 2 0nanostructures, J. Phys. Chem. Lett. 1 (19) (2010) 2837–2843.
[17] D. Gomez, K. Vernon, P. Mulvaney, T. Davis, Surface plasmon mediated strong exciton– photon coupling in semiconductor nanocrystals, Nano Lett. 10 (1) (2009) 274–278.
[18] N.T. Fofang, T.-H. Park, O. Neumann, N.A. Mirin, P. Nordlander, N.J. Halas, Plexcitonic nanoparticles: plasmon– exciton coupling in nanoshell– J-aggregate complexes, Nano Lett. 8 (10) (2008) 3481–3487.
[19] N.T. Fofang, N.K. Grady, Z. Fan, A.O. Govorov, N.J. Halas, Plexciton dynamics: exciton– plasmon coupling in a J-aggregate– Au nanoshell complex provides a mechanism for nonlinearity, Nano Lett. 11 (4) (2011) 1556–1560.
[20] Y.V. Bludov, M. Vasilevskiy, ATR Excitation of Surface Polaritons at the Interface between a Metal and a Layer of Nanocrystal Quantum Dots, 2011. Available from: arXiv preprint <arXiv:11022320>.
[21] W. William L.Q. Yu, Wenzhuo Guo, Xiaogang Peng, ChemMater 15 (2003) 2854–2860.
[22] K. Easawi MN, T. Abdallah, S. Negm, H. Talaat, Proc. World Acad. Sci. Eng. Technol. 61 (2012) 548–551.
[23] I. López, A. Vázquez, I. Gómez, Microwave assisted synthesis of CdS nanoparticles and their size evolution, Revista mexicana de física 59 (2) (2013) 160–164.
[24] P. Törmä, W.L. Barnes, Strong coupling between surface plasmon polaritions and emitters: a review, Rep. Prog. Phys. 78 (1) (2014) 013901.
[25] J. Ma, PacoZn, Capped by trioctylphosphine oxide (TOPO) Jo, University of Technology—Materials Science Edition v, 4p, 2011. Dichloro (bis [diphenylthiourea]) cadmium complex as a precursor for HDA-capped CdS nanoparticles and their solubility in water. South African J. Sci. (2010) 106 (7–8) 1–7.
[26] X. Nie, J. Xu, J. Cui, B. Yang, W. Jiang, Encapsulation of semiconductor quantum dots into the central cores of block copolymer cylindrical and toroidal micelles, RSC Adv. 3 (46) (2013) 24625–24633.
[27] J.K. Lorenz, A.B. Ellis, S-si, cadmium potpob, a sbaoT-n-ooa, nanocrystal posawrt, stabilization JotACS, vol. 120, no. 42, pp. 1998.
[28] D.C. Onwudiwe, C.A. Strydom, Tba, Cd(II); oN-pcoZla, synthesis s, thermal decomposition studies and use as, precursors for ZnS and CdS nanoparticles SA, Part A: Molecul. Biomolecul. Spectrosc. v (2015) 1080–1089.
[29] M. Chen Y.-G. Feng, X. Wang, T.-C. Li, J.-Y. Zhang, D.-J. Qian, Sncbof, growth as-o, Langmuir 23(10) (2007) pp. 5296–5304.
[30] D.C. Onwudiwe, M. Hrubaru, E.E. Ebenso, Synthesis, structural and optical properties of TOPO and HDA capped cadmium sulphide nanocrystals, and the effect of capping ligand concentration, J. Nanomater. 16 (1) (2015) 305.